# Chapter 3

# Functional Potential of the Core Phosphorelay Architecture

In this chapter, we ask how multiple phosphorelay inputs affect its bandpass characteristics, and, at a more basic level, how phosphotransfer reactions modulate signaling properties inside cells. We address these questions using simple computational models of two-component system architectures. Our results show that the two different types of phosphorelay inputs can be used to independently tune the two bandpass thresholds. Further, we note how the basic phosphotransfer reaction can be used as a building block for linear amplifier-like responses. These results provide broad correlations with design choices in electrical circuits, suggesting that similar considerations have governed the evolution of this architectural diversity.

## 3.1 Independent Tuning of Bandpass Thresholds

Phosphatases in two-component signaling circuits typically act on the proteins with a receiver domain, and the phosphorelay, with two such proteins, allows the possibility of two phosphatases acting on distinct protein components (Fig. 3.1a). Indeed, the phosphorelay regulating sporulation in *B. subtilis* utilizes this option and has phosphatases that act on Spo0A and Spo0F. Both phosphatases remove phosphates from the relay and are expected to have inhibitory effects on the phosphorelay output Spo0A$\sim$P. In this section, we analyze the effect of their structurally different points of action on the post-translational bandpass. We find that the two phosphatase types shift the bandpass in opposite directions and tune different bandpass thresholds (Fig. 3.1b).

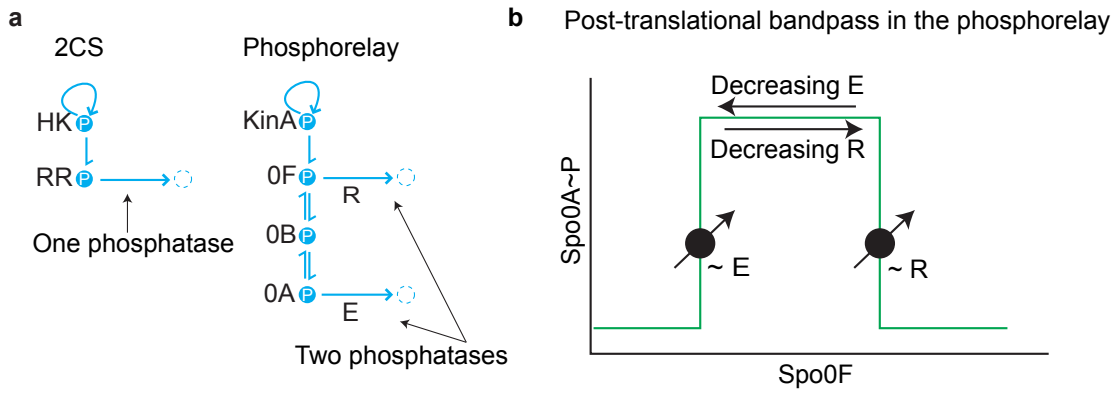


Figure 3.1: Effect of two types of phosphatases on the post-translational bandpass. (a) Canonical two-component system architecture with a histidine kinase (HK) and a response regulator (RR). Phosphorelay architecture with two phosphatases acting on Spo0A and Spo0F, denoted E and R, respectively. (b) Schematic of the effect of modulating phosphatase activities on the post-translational bandpass.

To show this, we used a simple mathematical model, already introduced in Sec. 2.2, to compute the post-translational bandpass response for different activities of the two phosphatases. In the post-translational bandpass response, Spo0A∼P levels are maximal at a unique value of total Spo0F concentration, dependent on the parameters of reaction rates and protein concentrations. For Spo0F levels higher than this value, the effective rate of reverse phosphotransfer away from Spo0A dominates, and diminishes the Spo0A∼P response (Fig. 2.4). The Spo0F phosphatase contributes to this effect by acting as a phosphate drain for the reverse flow of phosphates (Fig. C.1). For simplicity, we assume that the only source of Spo0F dephosphorylation is a phosphatase external to the phosphorelay ($k_h = 0$). This assumption allows a comparison of the two phosphatase activities without the complicating factor of the phosphatase activity of the kinase. Even with this assumption, the post-translational bandpass response is present in this model (Fig. 3.2, green line), and converts to a highpass response in the absence of a Spo0F phosphatase (Fig. 3.2, thick blue line). As expected from this, when the bandpass response is computed for different activities of the Spo0F phosphatase, it shifts towards higher Spo0F values (Fig. 3.2, thin blue lines).

Conversely, for Spo0F levels lower than this value, the effective rate of forward phosphotransfer to Spo0A is limiting, consistent with the notion that Spo0F is essential for phosphates to reach Spo0A. Interestingly, we find that in the absence of the Spo0A phos-

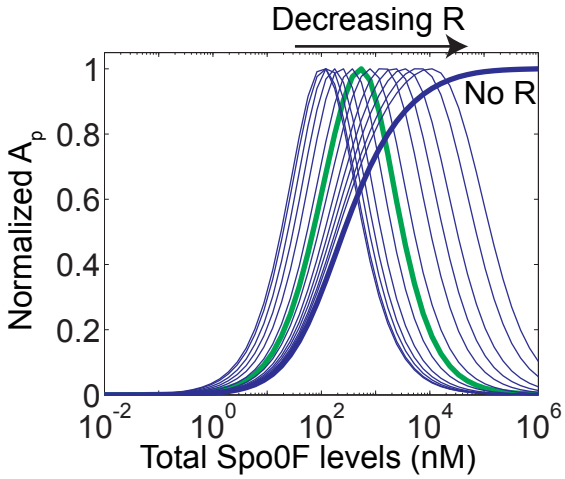


Figure 3.2: Decreasing Spo0F phosphatase activities shift the bandpass response towards higher Spo0F levels. Green line is the post-translational bandpass response curves from the model of the core phosphorelay. Thick blue line is the highpass response in the absence of a Spo0F phosphatase (denoted R, $k_r = 0$). Thin blue lines are bandpass response curves for different values of Spo0F phosphatase activity ($k_r = 10^4/hr$, $k_r = 5 \times 10^3/hr$, $k_r = 2 \times 10^3/hr$, $k_r = 10^3/hr$, $k_r = 5 \times 10^2/hr$, $k_r = 2 \times 10^2/hr$, $k_r = 50/hr$, $k_r = 20/hr$, $k_r = 10/hr$, $k_r = 5/hr$, $k_r = 2/hr$, $k_r = 1/hr$). In each case, the output $A_p$ is normalized by its maximum level.

phatase, low levels (non-zero) of Spo0F do not limit Spo0A∼P levels, and the response is purely lowpass (Fig. 3.3a, thick red line). This behavior can be understood by considering how phosphates are distributed in the Spo0F-Spo0B-Spo0A part of the phosphorelay model, and how phosphate input to the Spo0F-Spo0B-Spo0A part depends on total Spo0F levels.

The distribution of phosphates depends only on the phosphotransfer rates and the Spo0A phosphatase activity, and is given by the following equation,

$$k_t F_p B - k_{-t} F B_p = k_t B_p A - k_{-t} B A_p = k_e A_p.$$

In the absence of the Spo0A phosphatase ($k_e = 0$), this reduces to

$$k_t F_p B - k_{-t} F B_p = k_t B_p A - k_{-t} B A_p = 0. \tag{3.1}$$

This equation can be solved to obtain the dependence of the fraction of phosphorylated

Spo0A on total Spo0F levels.

$$
\begin{aligned}
& k_t B_p A - k_{-t} B A_p = 0, \\
\Longrightarrow \quad & k_t B_p A = k_{-t} B A_p, \\
\Longrightarrow \quad & k_t B_p (A_T - A_p) = k_{-t} B A_p, \\
\Longrightarrow \quad & k_t B_p A_T = (k_t B_p + k_{-t} B) A_p, \\
\Longrightarrow \quad & A_p = A_T \tfrac{k_t B_p}{k_t B_p + k_{-t} B}, \\
\Longrightarrow \quad & \tfrac{A_p}{A_T} = \tfrac{\frac{B_p}{B_T}}{\frac{B_p}{B_T} + \frac{k_{-t}}{k_t}(1 - \frac{B_p}{B_T})}.
\end{aligned} \tag{3.2}
$$

This equation expresses Spo0A∼P in terms of Spo0B∼P. In a similar fashion, Eq. (3.1) can be used to express Spo0B∼P in terms of Spo0F∼P.

$$
\begin{aligned}
& k_t F_p B - k_{-t} F B_p = 0, \\
\Longrightarrow \quad & k_t F_p B = k_{-t} F B_p, \\
\Longrightarrow \quad & k_t F_p (B_T - B_p) = k_{-t} F B_p, \\
\Longrightarrow \quad & k_t F_p B_T = (k_t F_p + k_{-t} F) B_p, \\
\Longrightarrow \quad & B_p = B_T \tfrac{k_t F_p}{k_t F_p + k_{-t} F}, \\
\Longrightarrow \quad & \tfrac{B_p}{B_T} = \tfrac{\frac{F_p}{F_T}}{\frac{F_p}{F_T} + \frac{k_{-t}}{k_t}(1 - \frac{F_p}{F_T})}.
\end{aligned} \tag{3.3}
$$

Together, Eqs. (3.2)–(3.3) can be rearranged to express Spo0A∼P in terms of Spo0F∼P.

$$
\frac{A_p}{A_T} = \frac{\frac{F_p}{F_T}}{\frac{F_p}{F_T} + (\frac{k_{-t}}{k_t})^2 (1 - \frac{F_p}{F_T}).} \tag{3.4}
$$

This expression shows that the fraction of phosphorylated Spo0A is a direct function of the fraction of phosphorylated Spo0F.

The phosphate input to the Spo0F-Spo0B-Spo0A part of the phosphorelay model depends on the balance between the phosphotransfer from KinA to Spo0F and the activity of the Spo0F phosphatase. This balance can be expressed as

$$
k_t K_p F = k_r F_p.
$$

For the given parameters, low Spo0F levels ($F_T << K_T$) mean that this phosphotransfer does not significantly deplete levels of KinA∼P, and is effectively a first-order reaction of Spo0F.

$$\begin{aligned} & K_p \approx K_T, \\ \Longrightarrow \quad & k_t K_T F \approx k_r F_p, \\ \Longrightarrow \quad & k_t K_T (F_T - F_p) \approx k_r F_p, \\ \Longrightarrow \quad & k_t K_T F_T \approx (k_t K_T + k_r) F_p, \\ \Longrightarrow \quad & \frac{F_p}{F_T} \approx \frac{k_t K_T}{k_t K_T + k_r}. \end{aligned} \tag{3.5}$$

Therefore, in this parameter regime, the fraction of phosphorylated Spo0F is independent of the total Spo0F levels. The combined effect of Eqs. (3.4)–(3.5) is that low levels of Spo0F do not affect the levels of Spo0A∼P. As expected from this, when the bandpass response is computed for decreasing Spo0A phosphatase activities, it shifts towards lower Spo0F values (Fig. 3.3a, thin red lines). These results show that the two phosphatases shift the bandpass response in opposite directions (Fig. 3.1b).

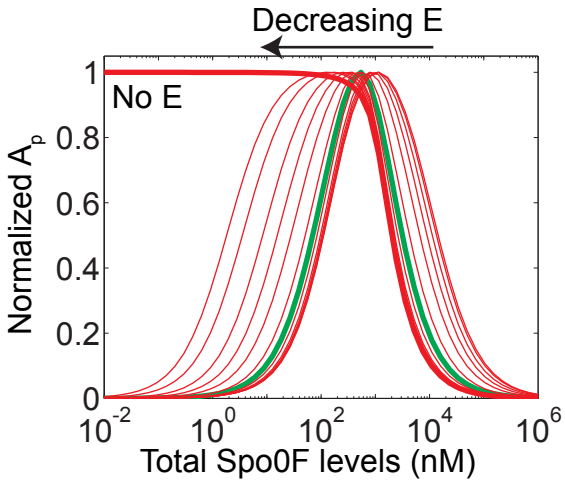


Figure 3.3: Decreasing Spo0A phosphatase activities shift the bandpass response towards lower Spo0F levels. Green line is the post-translational bandpass response curves from the model of the core phosphorelay. Thick red line is the highpass response in the absence of a Spo0A phosphatase (denoted E, $k_e = 0$). Thin red lines are bandpass response curves for different values of Spo0A phosphatase activity ($k_e = 10^4/hr$, $k_e = 5 \times 10^3/hr$, $k_e = 2 \times 10^3/hr$, $k_e = 10^3/hr$, $k_e = 5 \times 10^2/hr$, $k_e = 2 \times 10^2/hr$, $k_e = 50/hr$, $k_e = 20/hr$, $k_e = 10/hr$, $k_e = 5/hr$, $k_e = 2/hr$, $k_e = 1/hr$). In each case, the output $A_p$ is normalized by its maximum level.

There is also a quantitative difference in how these two phosphatases affect the thresholds of the post-translational bandpass response in the above computations. The shift in the higher bandpass threshold as the Spo0F phosphatase activity is varied is an order of magnitude more than the shift in the lower bandpass threshold (Fig. 3.4a). In addition, the shift in the lower bandpass threshold is for bandpasses with low amplitude. Based on these considerations, we conclude that the Spo0F phosphatase exerts a dominant effect on the higher bandpass threshold. Similarly, the shift in the lower bandpass threshold as the Spo0A phosphatase activity is varied is an order of magnitude more than the shift in the higher bandpass threshold (Fig. 3.4b). Further, the shift in the higher bandpass threshold is for bandpasses with low amplitude, suggesting that the Spo0A phosphatase exerts a dominant effect on the lower bandpass threshold. These results show that the two types of phosphatases provide almost independent parameters to tune the two bandpass thresholds (Fig. 3.1b). The presence of these independent tuning knobs is a direct consequence of the phosphorelay architecture.

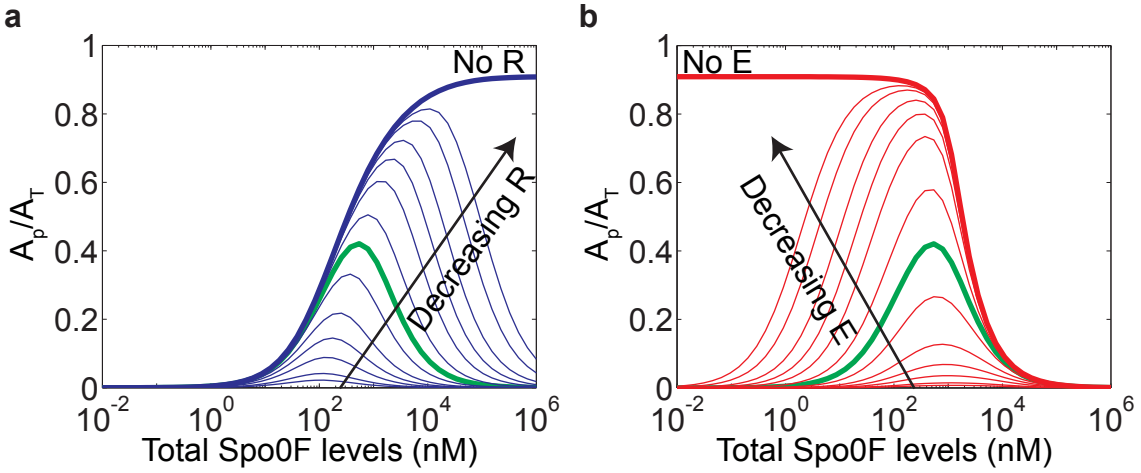


Figure 3.4: Two phosphatases in the phosphorelay independently tune the two thresholds of the post-translational bandpass response. Reproduction of bandpass curves from (a) Fig. 3.2 and (b) Fig. 3.3, with the output $A_p$ normalized by the total protein concentration $A_T$.

**Effect of phosphatase activity of KinA.** The above computations assume that Spo0F is dephosphorylated only by an external phosphatase and not by KinA ($k_h = 0$). To understand how the phosphatase activity of KinA affects the dependence of the bandpass response on the phosphorelay phosphatases, we repeated the above computations for two additional cases. First, we examined this dependence when the only source of Spo0F

dephosphorylation is KinA. This allows us to check if the conclusions in the above computations are critically dependent on the assumption $k_h = 0$. Second, we examined whether the phosphatase activity of KinA alters the dependence of the bandpass on the external phosphatases. This allows us to understand the effect of this interaction on the above conclusions.

We find that the bandpass response persists even when the only source of Spo0F dephosphorylation is the phosphatase activity of KinA ($k_r = 0$, Fig. 3.5a, green line), and converts to a highpass response when this is turned off ($k_h = 0$, Fig. 3.5a, thick blue line). As expected from this, when the bandpass response is computed for different phosphatase activities of KinA, it shifts towards higher Spo0F values (Fig. 3.5a, thin blue lines). Further, the shift in the lower bandpass threshold is for bandpasses with low amplitude (Fig. 3.5b). In other words, the phosphatase activity of KinA also exerts a dominant effect on the higher bandpass threshold. These results show that the dependence of the bandpass response on Spo0F phosphatase activity is similar irrespective of whether the source of dephosphorylation is KinA or an external Spo0F phosphatase.

We also checked the dependence of the bandpass response on Spo0A phosphatase activity when Spo0F is dephosphorylated only by KinA. We find that the bandpass response converts to a lowpass response in the absence of the Spo0A phosphatase, and that decreasing Spo0A phosphatase activities shift the bandpass towards lower Spo0F values (Fig. 3.6a). Further, the shift in the higher bandpass threshold is for bandpasses with low amplitude (Fig. 3.6b). In other words, the dominant effect of the Spo0A phosphatase is still on the lower bandpass threshold. As these features are similar to those noted previously (Fig. 3.3), we conclude that the effect of the Spo0A phosphatase activity on the bandpass is also similar irrespective of whether Spo0F is dephosphorylated by KinA or by an external phosphatase.

Next, we considered the modulation of the bandpass by the external phosphatases in the presence of the dephosphorylation of Spo0F by KinA. As both modes of Spo0F dephosphorylation — KinA and external — can regulate the bandpass location and threshold, we expect their relative contribution to determine the extent to which the external phosphatase can modulate these bandpass properties. When the phosphatase activity of KinA is low, the effect of the external Spo0F phosphatase is expected to be similar to the case considered previously, where KinA is not a phosphatase for Spo0F (Fig. 3.2, 3.4a). We find that this is indeed the case (Fig. 3.7a,b). As before, decreasing the activity of the

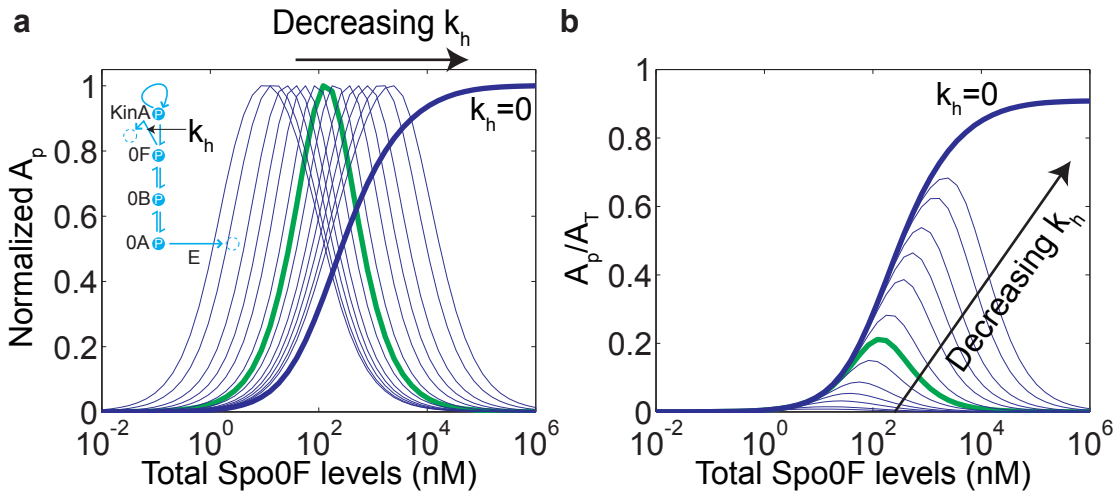


Figure 3.5: Decreasing the phosphatase activity of KinA shifts the bandpass towards higher Spo0F values and exerts a dominant effect on the higher bandpass threshold. (a) Green line is the post-translational bandpass response curves from the model of the core phosphorelay where the only source of Spo0F dephosphorylation is KinA ($k_r = 0$). Legend $k_h$ on the phosphorelay inset denotes this interaction. Thick blue line is the highpass response observed in the absence of this phosphatase activity ($k_h = 0$). Thin blue lines are bandpass response curves for different phosphatase activities of KinA ($k_h = 10^2/(nM \cdot hr)$, $k_h = 50/(nM \cdot hr)$, $k_h = 20/(nM \cdot hr)$, $k_h = 10/(nM \cdot hr)$, $k_h = 5/(nM \cdot hr)$, $k_h = 2/(nM \cdot hr)$, $k_h = 0.5/(nM \cdot hr)$, $k_h = 0.2/(nM \cdot hr)$, $k_h = 0.1/(nM \cdot hr)$, $k_h = 0.05/(nM \cdot hr)$, $k_h = 0.02/(nM \cdot hr)$, $k_h = 0.01/(nM \cdot hr)$). In each case, the output $A_p$ is normalized by its maximum level. (b) Bandpass response curves from (a) are replotted with the output $A_p$ normalized by the total protein concentration $A_T$.

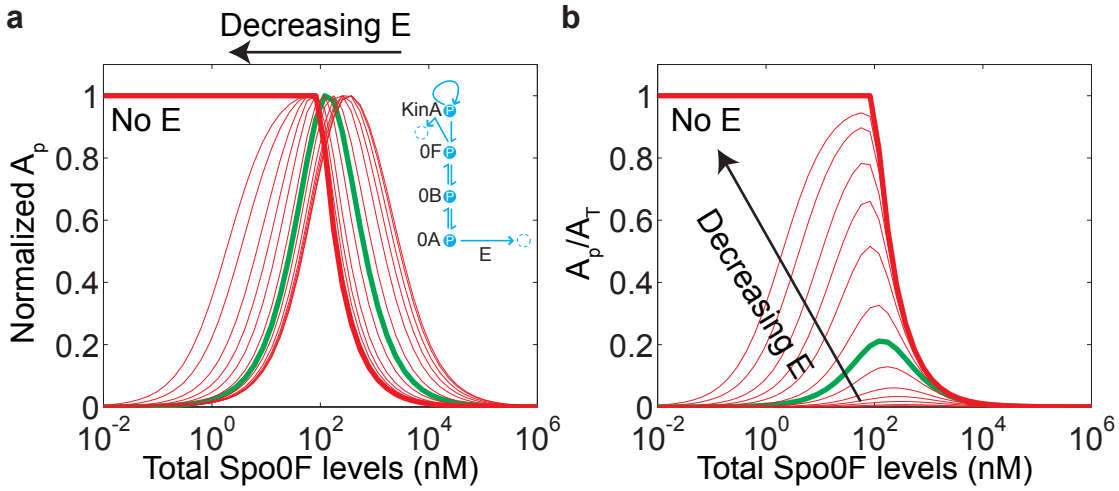


Figure 3.6: Decreasing Spo0A phosphatase activities shift the bandpass response towards lower Spo0F levels and exert a dominant effect on the lower bandpass threshold even when Spo0F is dephosphorylated by KinA. (a) Green line is the post-translational bandpass response curves from the model of the core phosphorelay where the only source of Spo0F dephosphorylation is KinA ($k_r = 0$). Thick red line is the highpass response in the absence of a Spo0A phosphatase (denoted E, $k_e = 0$). Thin red lines are bandpass response curves for different values of Spo0A phosphatase activity ($k_e = 10^4/hr$, $k_e = 5 \times 10^3/hr$, $k_e = 2 \times 10^3/hr$, $k_e = 10^3/hr$, $k_e = 5 \times 10^2/hr$, $k_e = 2 \times 10^2/hr$, $k_e = 50/hr$, $k_e = 20/hr$, $k_e = 10/hr$, $k_e = 5/hr$, $k_e = 2/hr$, $k_e = 1/hr$). In each case, the output $A_p$ is normalized by its maximum level. (b) Bandpass response curves from (a) are replotted with the output $A_p$ normalized by the total protein concentration $A_T$.

external Spo0F phosphatase shifts the bandpass towards higher Spo0F values (Fig. 3.7a). Further, the external Spo0F phosphatase continues to exert a dominant effect on the higher bandpass threshold (Fig. 3.7b). A minor difference, however, is that bandpass does not convert into a highpass response when the external Spo0F phosphatase activity is turned off (Fig. 3.7a, thick blue line). This is along expected lines as a bandpass will exist as long as there is dephosphorylation of Spo0F, which in this case is through KinA. In contrast, when the phosphatase activity of KinA is high, we find that the external Spo0F phosphatase has little effect on the bandpass location or threshold (Fig. 3.7c,d). This is because the principal contribution to the net Spo0F phosphatase activity, which modulates these bandpasss properties, is through KinA and not the external phosphatase. Therefore, the modulation of the bandpass location and threshold by an external Spo0F phosphatase is effective when the phosphatase activity of KinA is low.

Finally, we note that the effect of the Spo0A phosphatase on the bandpass doesn't depend significantly on the strength of the KinA phosphatase (Fig. 3.8), and is similar to the cases considered previously (Figs. 3.3, 3.4b and 3.6).

## 3.2 Linear Amplifier-like Responses

In this section, we investigate the role of the phosphotransfer reaction in modulating the input-output response. We characterize its effect on the sensitivity ($s$) of response, estimated by the relative change of output ($y$) with respect to the input ($x$). The sensitivity can be obtained by computing the logarithmic derivative of the input-output response,

$$s = \frac{\partial \log y}{\partial \log x}.$$

This measure highlights the difference between a switch-like response and an amplifier-like response (Fig. 3.9). For a switch-like response, the sensitivity is extremely high near the switching threshold and very small away from this threshold. In contrast, the sensitivity for an amplifier-like response is constant throughout the range of input/output. We find that the phosphotransfer reaction can increase the range of sensitivity of the response, allowing two-component systems to operate as signaling amplifiers.

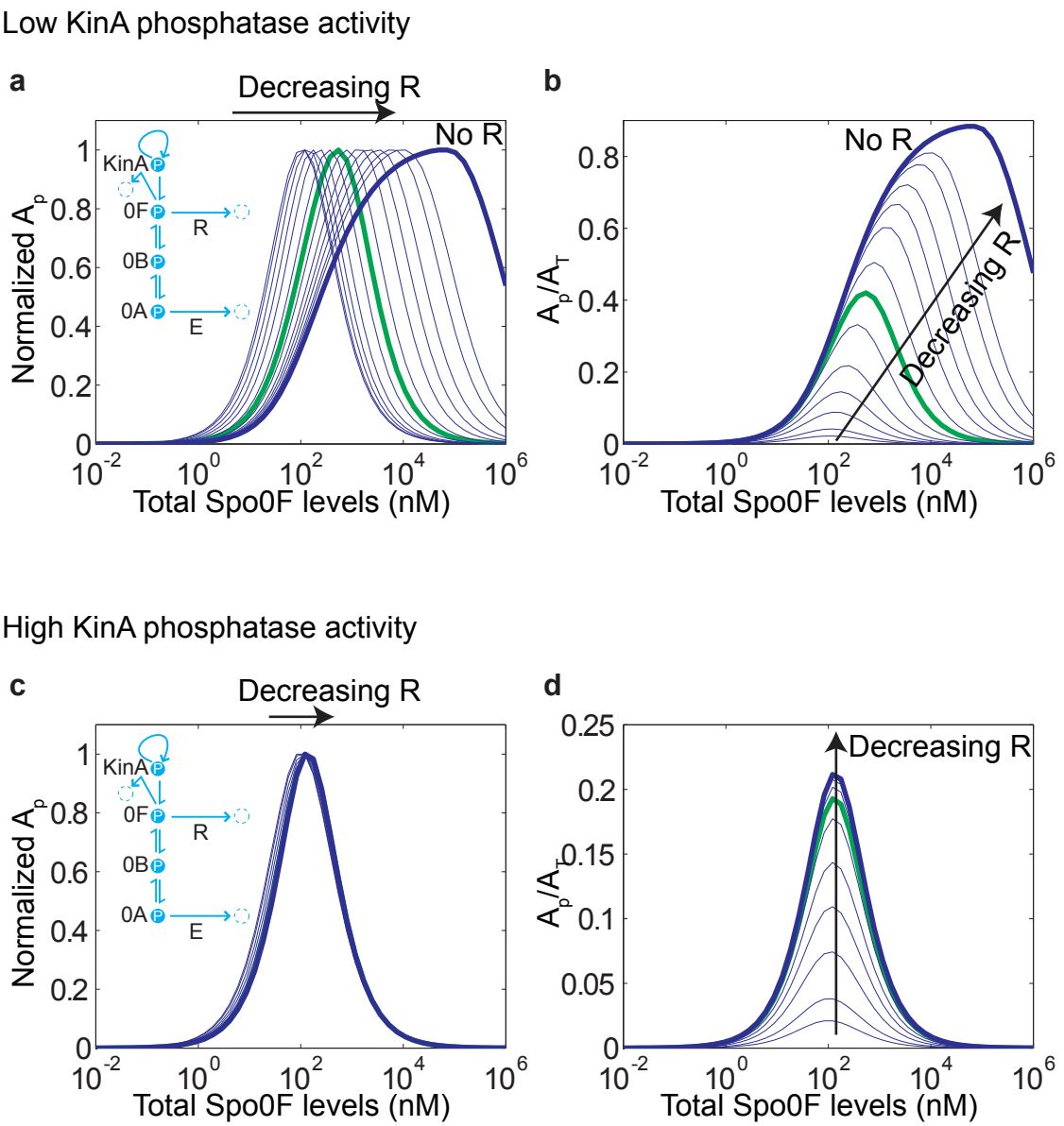


Figure 3.7: Bandpass regulation by external Spo0F phosphatase activity depends on the phosphatase activity of KinA. (a) Green line is the bandpass response from the model of the core phosphorelay with a low phosphatase activity of KinA ($k_h = 1 \times 10^{-4}/(nM \cdot hr)$). Thick blue line is the bandpass response in the absence of an external Spo0F phosphatase (denoted R, $k_r = 0$). Thin blue lines are bandpass response curves for different values of the external Spo0F phosphatase activity ($k_r = 10^4/hr$, $k_r = 5 \times 10^3/hr$, $k_r = 2 \times 10^3/hr$, $k_r = 10^3/hr$, $k_r = 5 \times 10^2/hr$, $k_r = 2 \times 10^2/hr$, $k_r = 50/hr$, $k_r = 20/hr$, $k_r = 10/hr$, $k_r = 5/hr$, $k_r = 2/hr$, $k_r = 1/hr$). In each case, the output $A_p$ is normalized by its maximum level. (b) Bandpass response curves from (a) are replotted with the output $A_p$ normalized by the total protein concentration $A_T$. (c) Bandpass response curves from (a) are replotted for a high phosphatase activity of KinA ($k_h = 1/(nM \cdot hr)$). (d) Bandpass response curves from (c) are replotted with the output $A_p$ normalized by the total protein concentration $A_T$.

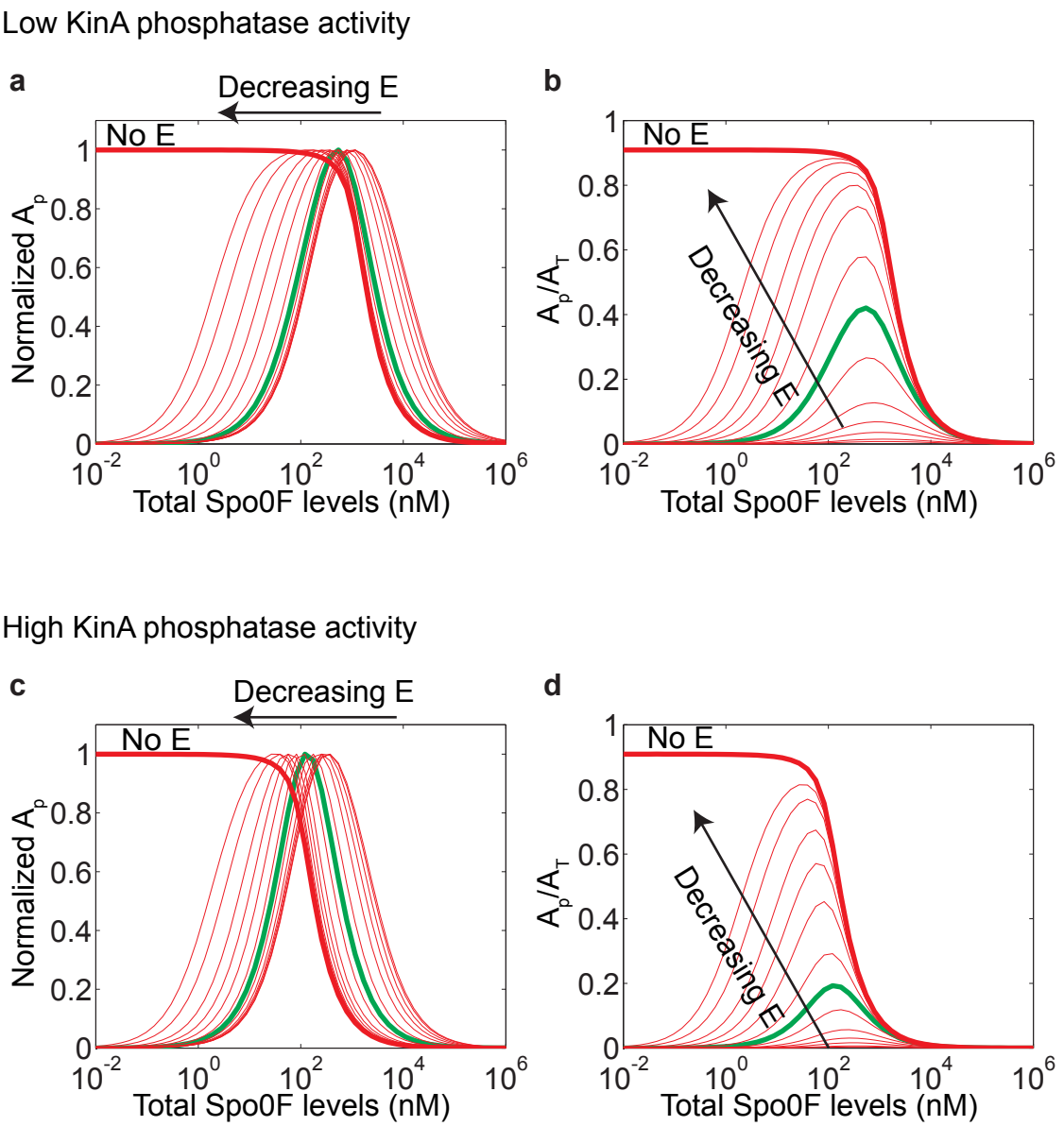


Figure 3.8: Bandpass regulation by Spo0A phosphatase activity does not significantly depend on the phosphatase activity of KinA. (a) Green line is the bandpass response from the model of the core phosphorelay with a low phosphatase activity of KinA ($k_h = 1 \times 10^{-4}/(nM \cdot hr)$). Thick red line is the highpass response in the absence of a Spo0A phosphatase (denoted E, $k_e = 0$). Thin red lines are bandpass response curves for different values of Spo0A phosphatase activity ($k_e = 10^4/hr$, $k_e = 5 \times 10^3/hr$, $k_e = 2 \times 10^3/hr$, $k_e = 10^3/hr$, $k_e = 5 \times 10^2/hr$, $k_e = 2 \times 10^2/hr$, $k_e = 50/hr$, $k_e = 20/hr$, $k_e = 10/hr$, $k_e = 5/hr$, $k_e = 2/hr$, $k_e = 1/hr$). In each case, the output $A_p$ is normalized by its maximum level. (b) Bandpass response curves from (a) are replotted with the output $A_p$ normalized by the total protein concentration $A_T$. (c) Bandpass response curves from (a) are replotted for a high phosphatase activity of KinA ($k_h = 1/(nM \cdot hr)$). (d) Bandpass response curves from (c) are replotted with the output $A_p$ normalized by the total protein concentration $A_T$.

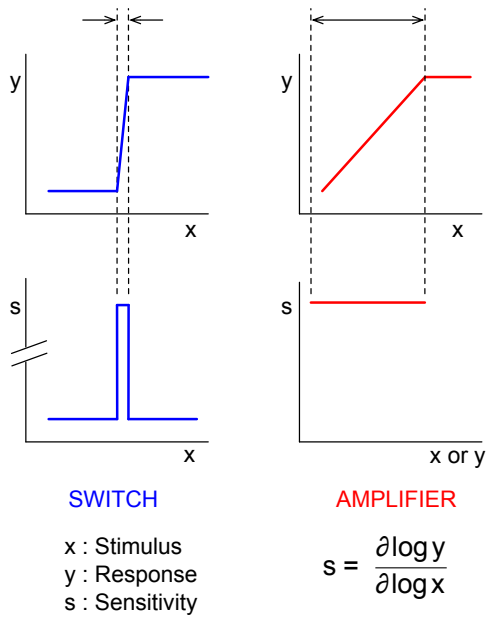


Figure 3.9: Idealized stimulus-response curves and sensitivity profiles of a switch (blue) and an amplifier (red).

### 3.2.1 Two-Component System

Before investigating the dependence of the two-component system sensitivity profiles on the phosphotransfer reaction, we introduce, for comparison purposes, a hypothetical one-component system model. The one-component system consists of a protein, whose phosphorylated form (denoted $R_p$) functions as the output response and the unphosphorylated form ($R$) is the input sensor. We model the response of a 1CS using the simple mass action kinetics,

$$\frac{dR_p}{dt} = k_s(R_T - R_p) - k_h R_p.$$

Here, $R_T = R + R_p$ is the total concentration, $k_s$ is the rate of phosphorylation that acts as the input stimulus, and $k_h$ is the rate of dephosphorylation. At steady state,

$$\frac{dR_p}{dt} = 0 \implies R_p = R_T \frac{k_s}{k_s + k_h}.$$

For this input-output response, the sensitivity can be expressed analytically as

$$s = \frac{\partial \log R_p}{\partial \log k_s} = \frac{k_h}{k_s + k_h} = 1 - \frac{R_p}{R_T}.$$

These expressions show that the sensitivity ($s$) decreases as the input ($k_s$) is increased, or, equivalently, as the output levels ($R_p$) increase (Fig. 3.10, black). Because the sensing and response functions are encoded on the same molecule, an increase in the output ($R_p$) automatically reduces the sensor levels ($R$). This consideration limits the range of linear sensitivity ($s \approx 1$) in a 1CS.

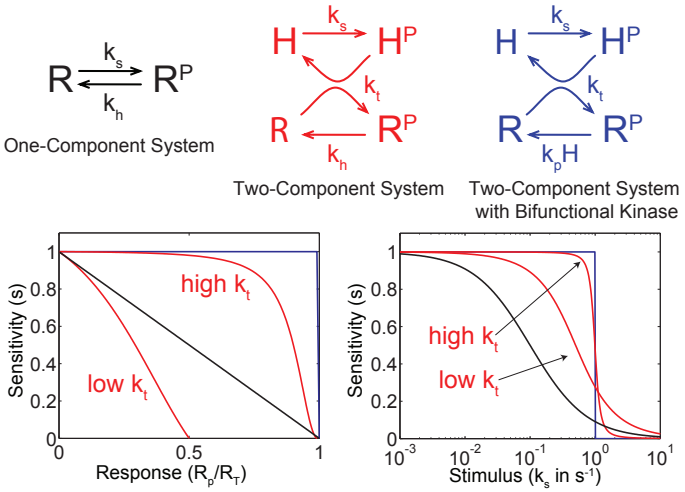


Figure 3.10: Phosphotransfer can enhance range of linear sensitivity. Black, red, and blue lines indicate the sensitivity profiles from models of the one-component system, the two-component system, and the two-component system with a bifunctional kinase, respectively. Parameters: $H_T$=10$nM$, $R_T$=$10^2 nM$, $k_h$=$10^{-1}s^{-1}$, $k_p$=$k_h/H_T$, low $k_t$=$10^{-2}/(nM \cdot s)$, high $k_t$=$10^0/(nM \cdot s)$.

Now, we compute the sensitivity in a two-component system model, in which the sensing and response functions necessarily reside on two separate protein components. The two-component system model has three reactions: autophosphorylation of the sensor kinase ($H$), phosphotransfer from the phosphorylated sensor kinase ($H_p$) to the response regulator ($R$), and dephosphorylation of the phosphorylated regulator ($R_p$),

$$\begin{aligned} \frac{dH_p}{dt} &= k_s(H_T - H_p) - k_t H_p(R_T - R_p), \\ \frac{dR_p}{dt} &= k_t H_p(R_T - R_p) - k_h R_p. \end{aligned}$$

Here, $H_T$ and $R_T$ are total concentrations, $k_s$ is the rate of autophosphorylation ( and the input stimulus), $k_t$ is the rate of phosphotransfer, and $k_h$ is the rate of dephosphorylation. For this model, the steady state condition results in a quadratic equation in $R_p$ that can be numerically solved to compute the input-output response ($R_p$ vs $k_s$) and the corresponding

sensitivity profile. We find that, in the limit of fast phosphotransfer ($k_t H_T > k_h$), the range of linear sensitivity in the input stimulus and in the output range is enhanced from that possible in a 1CS (Fig. 3.10, red). This is because rapid phosphotransfer shuttles phosphates away from the sensor ($H_p$) to the response regulator ($R$), thereby freeing up sensor ($H$) to detect further changes in input.

Next, we investigated the role of a bifunctional kinase on the response sensitivity. For this we augmented the two-component system model so that the dephosphorylation of the response regulator is mediated by the unphosphorylated sensor kinase ($H$),

$$\begin{aligned} \frac{dH_p}{dt} &= k_s(H_T - H_p) - k_t H_p(R_T - R_p), \\ \frac{dR_p}{dt} &= k_t H_p(R_T - R_p) - k_p(H_T - H_p)R_p. \end{aligned}$$

Here, $k_h$ is the rate of kinase-dependent dephosphorylation of the response regulator. The steady state input-output response for this model is

$$R_p = \begin{cases} \frac{k_s}{k_p} & \text{if } k_s < k_p R_T, \\ R_T & \text{if } k_s > k_p R_T. \end{cases}$$

The sensitivity of this response is

$$s = \begin{cases} 1 & \text{if } k_s < k_p R_T, \\ 0 & \text{if } k_s > k_p R_T. \end{cases}$$

Therefore, the response in this model is perfectly linear as long as it is unsaturated (Fig. 3.10, blue). The linear response in the model of a two-component system with a bifunctional kinase is consistent with the trend of linear sensitivity discussed for the two-component system model.

### 3.2.2 Phosphorelay

Based on the increased range of linear sensitivity with the addition of a single rapid phosphotransfer step, it is reasonable to expect a further enhancement with a cascade of similarly rapid phosphotransfer steps. To test this, we augmented the two-component system model

with the addition of two more protein components to make a four-component system model. In the four-component system model, phosphate is transferred sequentially from the sensor kinase ($H$) to the response regulator ($R$) via intermediatory proteins $T$ and $D$,

$$\begin{aligned}
\frac{dH_p}{dt} &= k_s(H_T - H_p) - k_t H_p(D_T - D_p), \\
\frac{dD_p}{dt} &= k_t H_p(D_T - D_p) - k_t D_p(T_T - T_p), \\
\frac{dT_p}{dt} &= k_t D_p(T_T - T_p) - k_t T_p(R_T - R_p), \\
\frac{dR_p}{dt} &= k_t T_p(R_T - R_p) - k_h R_p.
\end{aligned}$$

Here, the steady state condition results in a quartic equation that can be numerically solved to obtain the input-output response and the corresponding sensitivity profile. For the same parameters as the two-component system model, we find that the sensitivity profile for this input-output response is linear for a larger range (Fig. 3.11). The enhanced linearity is because each stage in the cascade shuttles phosphate to the next stage, thereby staying free (unphosphorylated) to detect further changes in the effective stage input. Therefore, we find that one consequence of phosphotransfer reactions is that they can enhance the range of linear sensitivity.

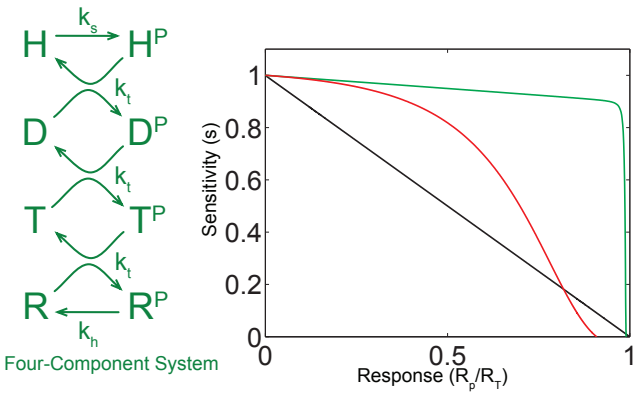


Figure 3.11: Phosphorelay can further increase the range of linear sensitivity. Sensitivity profiles of a one-component system (red), a two-component system (black), and a four-component system (green). Four-component system parameters: $H_T$=$10nM$, $R_T$=$10^2nM$, $k_h$=$10^{-1}s^{-1}$, $k_t$=$10^{-1}/(nM \cdot s)$, $D_T$=$T_T$=$R_T$.

Linear input-output response in a similar phosphorelay model has been recently reported [15]. The approach used is complementary to the one presented here, and focuses

on comparison of the signaling response across different stages of the phosphorelay.

**Robustness of the output to protein concentrations.** These results present an investigation of the input-output sensitivity of some two-component signaling architectures. Another signaling property that has the potential to be functionally useful is the robustness of the output to changes in concentrations of the protein components. In fact, previous investigations of this in the context of the two-component system with a bifunctional kinase have noted that the output can be robust to the concentrations of the response regulator and of the kinase [7, 51, 54]. Here, we examine the presence of this robustness property in the models discussed above. We note that this robustness property is also present in the model of the two-component system with a bifunctional kinase described here. In particular, there are two regimes in this model (Fig. 3.12a): one, at low $R_T$ levels, where the output is saturated and so depends on $R_T$, and two, at high $R_T$ levels, where the output is independent of $R_T$. The steady state output values in this figure are computed by numerically integrating the model equations for increasing levels of $R_T$. Robustness to a parameter requires integral feedback attenuating the effect of that parameter, and the phosphatase activity of the kinase has been identified as a key element of the feedback mechanism providing robustness to changes in protein concentrations [54]. It is illustrative to compare this behavior with that of the one-component system model. In this case, the output is not robust to $R_T$ (Fig. 3.12b, generated by numerical integration). Therefore, there is no feedback in this model that makes the output robust to changes in the concentration of the response regulator.

Motivated by the existence of this robustness property in the two-component model with a bifunctional kinase, we examined its existence in the model of the simple two-component system architecture, where the kinase does not possess the phosphatase activity. To investigate this, we computed the steady state output values by numerically integrating the equations for increasing levels of $R_T$. We find a robustness property that is similar to the one in the model with a bifunctional kinase (Fig. 3.12c): at low $R_T$ levels, the output is dependent on $R_T$, and at high $R_T$ levels, the output is largely independent of $R_T$. While the transition between these two regimes is not as sharp as the one in the model with a bifunctional kinase, there is a regime where the output is almost robust to the concentration of the response regulator. The only difference between this model and the one-component system model, which doesn't have this robustness property, is the phosphotransfer reaction. This suggests that phosphotransfer is a key element of the feedback mechanism providing

robustness to $R_T$. We find that the four-component system model, which has a cascade of phosphotransfers, also has this robustness property (Fig. 3.12d, generated by numerical integration). Similar output robustness properties also exist with respect to the concentration of the histidine kinase in the models of two-component system with the bifunctional kinase (see also [7, 51, 54]), the simple two-component system, and the four-component system (Fig. 3.13), as well as with respect to the other phosphotransfer proteins in the four-component system model (Fig. 3.14). Therefore, these models of two-component system architectures have regimes where the output is robust to the protein concentrations.

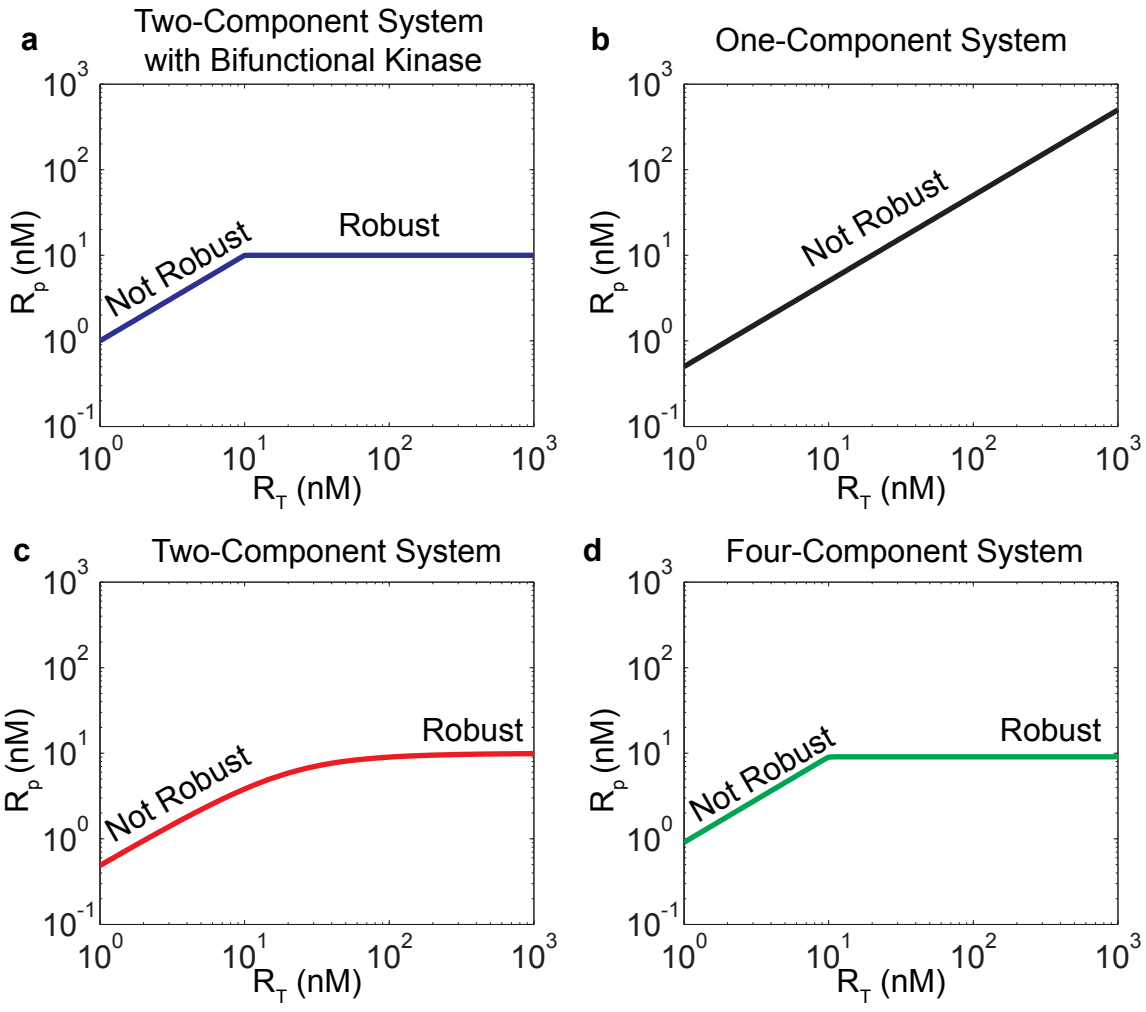


Figure 3.12: Output can be robust to $R_T$ in two-component system architectures. Dependence on the output ($R_p$) on the concentration of the response regulator ($R_T$) for models of (a) two-component system with a bifunctional kinase, (b) one-component system, (c) two-component system, and (d) four-component system. Parameters: $H_T$=10$nM$, $D_T$=$T_T$=$10^2 nM$, $k_h$=$10^{-1} s^{-1}$, $k_p$=$k_h/H_T$, $k_t$=$10^{-2}/(nM \cdot s)$.

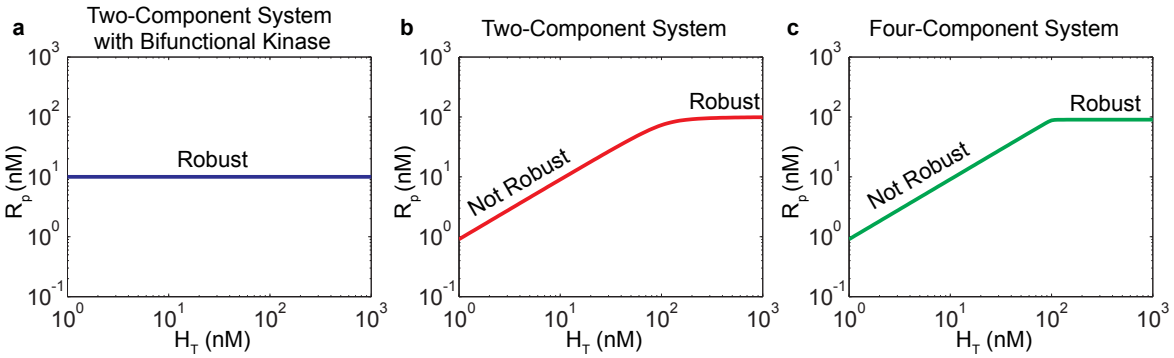


Figure 3.13: Output can be robust to $H_T$ in two-component system architectures. Dependence on the output ($R_p$) on the concentration of the histidine kinase ($H_T$) for models of (a) two-component system with a bifunctional kinase, (b) two-component system, and (c) four-component system. Parameters: $H_T$=$10nM$, $R_T$=$D_T$=$T_T$=$10^2nM$, $k_h$=$10^{-1}s^{-1}$, $k_p$=$10^{-2}/(nM\cdot s)$, $k_t$=$10^{-2}/(nM\cdot s)$.

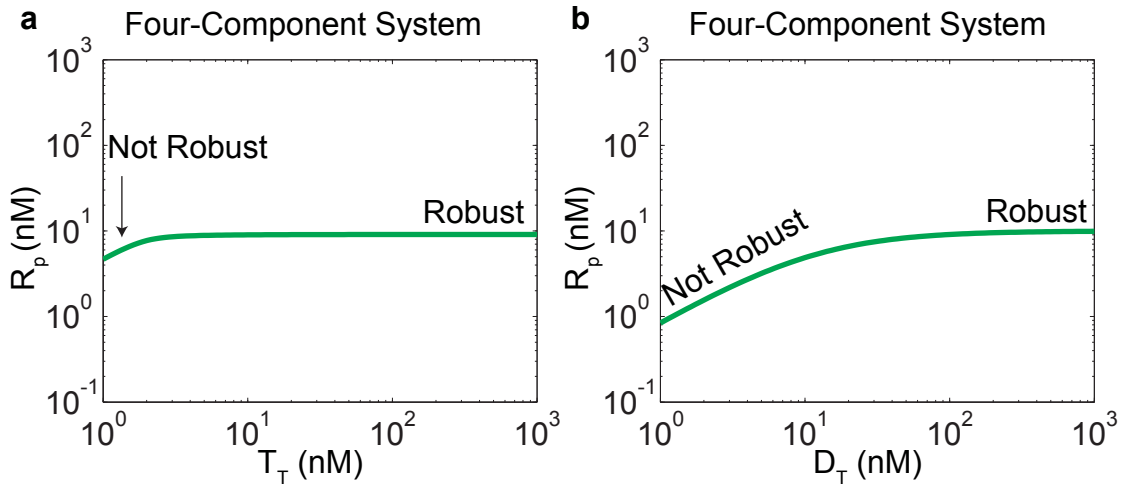


Figure 3.14: Output can be robust to intermediatory phosphotransfer proteins in the four-component system architecture. Dependence on the output ($R_p$) in the four-component system model on (a) the concentration of $T_T$ for $D_T$=$10^2nM$ and (b) the concentration of $D_T$ for $T_T$=$10^2nM$. Other parameters: $H_T$=$10nM$, $R_T$=$10^2nM$, $k_h$=$10^{-1}s^{-1}$, $k_t$=$10^{-2}/(nM\cdot s)$.

**Phosphotransfer reactions in hybrid architectures can enhance the range of ultrasensitivity.** Phosphotransfer reactions analyzed so far have been intermolecular, from one protein to another. Additionally, phosphotransfer can also occur intramolecularly, between two domains of the same protein. Signaling architectures with such hybrid proteins are called hybrid architectures. To understand how phosphotransfer reactions affect signaling properties of hybrid phosphorelays, we computed their input-output responses. Some aspects of the reaction mechanisms in the hybrid proteins are not clearly known. For example, consider a hypothetical two-component system architecture consisting of a hybrid kinase AB, and a response regulator C. It is not clear if all possible phosphoforms — $AB$, $A_pB$, $AB_p$, $A_pB_p$ — exist. Assuming they do, it is not clear whether the phosphoforms ($AB_p$, $A_pB_p$) are equally capable of phosphotransfer to $C$. Consequently, certain additional assumptions are required before computing the input-output response.

To analyze the response sensitivity here, we first assumed that the phosphoform $A_pB_p$ exists and is the only state that transfers phosphates to $C$ (Fig. 3.15). This reaction scheme has three types of reactions: autophosphorylation of $AB$ and $AB_p$, phosphotransfer from $A_pB$ to $AB_p$ and from $A_pB_p$ to $C$, and dephosphorylation of $AB_p$ and $C_p$,

$$\begin{aligned}
\frac{d[A_pB]}{dt} &= k_s(AB_T - [A_pB] - [AB_p] - [A_pB_p]) - k_t[A_pB] + k_1C[A_pB_p], \\
\frac{d[AB_p]}{dt} &= -k_2[AB_p] + k_t[A_pB] - k_s[AB_p], \\
\frac{d[A_pB_p]}{dt} &= -k_2[AB_p] + k_t[A_pB] - k_s[AB_p], \\
\frac{dC_p}{dt} &= k_1C[A_pB_p] - k_hC_p.
\end{aligned}$$

Here, $AB_T$ and $C_T$ are total concentrations, $k_s$ is the rate of autophosphorylation (and the input stimulus), $k_t$ is the rate of phosphotransfer from $A_pB$ to $AB_p$, $k_1$ is the rate of phosphotransfer from $A_pB_p$ to $C$, $k_2$ is the rate of dephosphorylation of $AB_p$, and $k_h$ is the rate of dephosphorylation of $C_p$. For this model, we use numerical integration to investigate the steady state input-output responses ($C_p$ vs $k_s$). We find that it is possible to generate an enhanced range of quadratic sensitivity (s≈2, Fig. 3.15), through a mechanism similar to the linear responses discussed above. This can be explained as follows: As the phosphoform $A_pB_p$ has two phosphates, it requires two cycles of input to reach it. This increases the maximum absolute sensitivity from 1, as in previous models, to 2. Next, a

rapid phosphotransfer rate can increase the range of this ultrasensitivity ($s > 1$) via the same phosphate-shuttling mechanism as in the models above. So, the quadratic sensitivity arises due to the multiple phosphorylation assumption and the extended range of quadratic sensitivity is due to rapid phosphotransfer. Therefore, this response is conceptually similar to the amplifier-like responses in models of 2CS architectures.

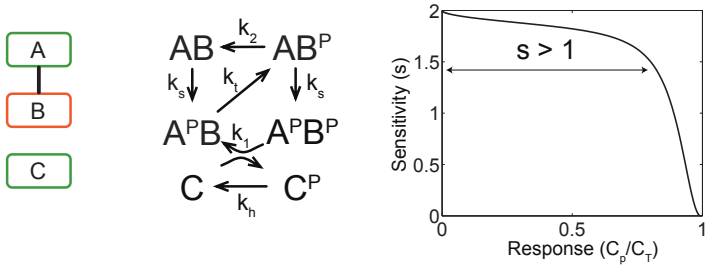


Figure 3.15: Enhanced range of quadratic sensitivity in a hybrid phosphorelay reaction scheme. Parameters for the response curve: $AB_T = 10nM$, $C_T = 100nM$, $k_t = 10s^{-1}$, $k_1 = 10^{-1}/(nM \cdot s)$, $k_2 = 10s^{-1}$, $k_h = 10^{-2}s^{-1}$, $k_s$ is varied in the range $10^{-3}s^{-1}$–$10^{1}s^{-1}$.

Next, we considered the case where the roles of the phosphoforms $AB_p$ and $A_pB_p$ are switched, so that $AB_p$ transfers phosphates to $C$ (Fig. 3.16). This reaction scheme has the same reactions as above, except for the phosphotransfer from $AB_p$ to $C$ and the dephosphorylation of $A_pB_p$,

$$\begin{aligned}
\frac{d[A_pB]}{dt} &= k_s(AB_T - [A_pB] - [AB_p] - [A_pB_p]) - k_t[A_pB] + k_1[A_pB_p], \\
\frac{d[AB_p]}{dt} &= -k_2C[AB_p] + k_t[A_pB] - k_s[AB_p], \\
\frac{d[A_pB_p]}{dt} &= -k_2C[AB_p] + k_t[A_pB] - k_s[AB_p], \\
\frac{dC_p}{dt} &= k_2C[A_pB_p] - k_hC_p.
\end{aligned}$$

Here, $k_2$ is the rate of phosphotransfer from $AB_p$ to $C$, and $k_1$ is the rate of dephosphorylation of $A_pB_p$. For this model, we use numerical integration to investigate the steady state input-output responses ($C_p$ vs $k_s$). We find that it is possible to generate a non-monotonic response (Fig. 3.16). This can be explained as follows: As stimulus levels increase, the phosphoform $AB_p$ is populated earlier than the phosphoform $A_pB_p$. For further increase in stimulus levels, all of the sensor kinase is in the $A_pB_p$ phosphoform and the population of $AB_p$ decreases. Therefore, the phosphoform $AB_p$ has a non-monotonic response to the

stimulus levels. As phosphotransfer is from $AB_p$ to $C$, this non-monotonic profile is reflected in the response regulator output. Therefore, a non-monotonic response is also possible in this hybrid kinase architecture.

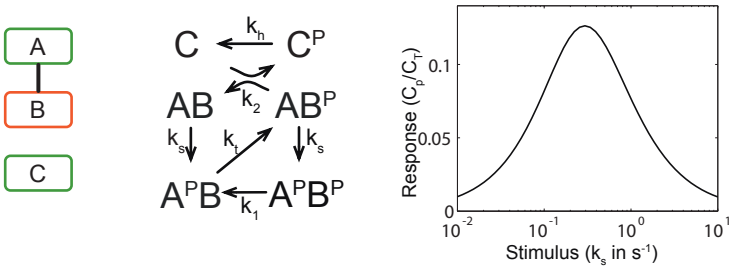


Figure 3.16: Non-monotonic response in a hybrid phosphorelay reaction scheme. Parameters for the reaction scheme: $AB_T = 10nM$, $C_T = 100nM$, $k_t = 10^0 s^{-1}$, $k_1 = 10^{-2} s^{-1}$, $k_2 = 10/(nM \cdot s)$, $k_h = 10^{-1} s^{-1}$.

## 3.3 Analogies to Electrical Circuits

Here, we have explored the functional potential of the phosphorelay, an architectural variant of the family of two-component system circuits. Using simple computational models, we find that: One, the two types of phosphatases in the phosphorelay can be used by the cell to shift the post-translational bandpass in different directions, and to independently tune its two thresholds in a quantitative fashion. Two, the phosphotransfer reaction, a basic building block of two-component system architectures, can be used to design linear signaling amplifiers. These results suggest ways in which cells can harness the functional potential of different two-component system architectures.

Tuning parameters are an important aspect of electrical circuits, typically used to optimize the design for different operating conditions. These can be used in static scenarios, such as in tuning bandpass thresholds to detect a band of voltage levels, or in dynamic scenarios, such as in tuning gains of adaptive controllers. In fact, response curves in electrical circuits used to detect voltage bands are analogous to the post-translational bandpass discussed above. Similarly, linearity in amplifier response can also be an important consideration in electrical circuits, as in sound systems, where deviations from linearity introduce distortion in the output. The requirement for linearity is especially important in cases where the input signal has a large dynamic range. In particular, simple linear amplifiers constructed

using electronic op-amps are analogous to two-component systems with linear amplifiers in their use of feedback. Negative feedback is used to generate linear input-output profiles in an electronic op-amp. In an analogous fashion, negative feedback, encoded via the phosphotransfer reaction, can enhance the range of linear sensitivity in simple two-component systems.

The consumption of power is a significant constraint in the design of electrical circuits. Given their broad analogies with electrical circuits, power consumption may also be a challenge in the evolution of two-component signaling circuits. It will be interesting to characterize the rates of power consumption across different two-component system architectures. This may highlight design tradeoffs in signaling circuits, and provide insights into the architectural diversity of two-component signaling systems.

Computational studies of signaling circuits can reveal properties that have the potential to be functionally used by the cell. Here, these properties include independent tuning parameters for different aspects of the response, as well as ways to generate linear amplifier-like responses. Juxtaposing these circuits against their distribution in various cellular contexts will be instructive in understanding if and how these properties are used. The growing number of two-component signaling circuits in bacteria being identified by recent genome sequencing and annotation efforts offers a useful starting point for this [65]. These data have already highlighted a correlation between the number of such signaling circuits and genome size [2], suggesting that these circuits are needed to encode complex signal processing tasks. This is also supported by the broad correlation that exists between the complexity of a phosphotransfer configuration and the enormity of the cellular function that it encodes [5]. Further investigations of how these circuits operate in their natural contexts may reveal other instances of potentially useful properties, and will be required to determine if such properties are essential or merely by-products of molecular interactions used to implement cellular signaling.